Monte Carlo study of anisotropic scaling generated by disorder

O. Vasilyev
Max-Planck-Institut für Intelligente Systeme, Heisenbergstraße 3, D-70569 Stuttgart, Germany
and IV. Institut für Theoretische Physik, Universität Stuttgart, Pfaffenwaldring 57, D-70569 Stuttgart, Germany

B. Berche
Statistical Physics Group, Institut Jean Lamour, UMR CNRS 7198
and Université de Lorraine, B.P. 70239, F-54506 Vandœuvre lès Nancy Cedex, France

M. Dudka and Yu. Holovatch
Institute for Condensed Matter Physics, National Academy of Sciences of Ukraine, UA-79011 Lviv, Ukraine
(Received 13 May 2015; revised manuscript received 10 September 2015; published 7 October 2015)

We analyze the critical properties of the three-dimensional Ising model with linear parallel extended defects. Such a form of disorder produces two distinct correlation lengths, a parallel correlation length $\xi_\parallel$ in the direction along defects and a perpendicular correlation length $\xi_\perp$ in the direction perpendicular to the lines. Both $\xi_\parallel$ and $\xi_\perp$ diverge algebraically in the vicinity of the critical point, but the corresponding critical exponents $\nu_\parallel$ and $\nu_\perp$ take different values. This property is specific for anisotropic scaling and the ratio $\nu_\parallel/\nu_\perp$ defines the anisotropy exponent θ. Until now, estimates of quantitative characteristics of the critical behavior for such systems have been obtained only within the renormalization group approach. We report a study of the anisotropic scaling in this system via Monte Carlo simulation of the three-dimensional system with Ising spins and nonmagnetic impurities arranged into randomly distributed parallel lines. Several independent estimates for the anisotropy exponent θ of the system are obtained, as well as an estimate of the susceptibility exponent γ. Our results corroborate the renormalization group predictions obtained earlier.

DOI: 10.1103/PhysRevE.92.042118 PACS number(s): 64.60.F−, 05.10.Ln, 75.10.Hk

I. INTRODUCTION

The effect of structural disorder on criticality remains one of the most attractive issues in condensed-matter physics [1]. Realistic systems always contain some imperfections of their structure. Thus the question of how disorder influences the critical properties of a system deserves considerable interest. Obviously the modifications introduced depend on the amount of disorder as well as on the type of disorder. Quenched disorder is usually studied in the form of dilution (random site [2] or random bond [3] systems) or as a random field [4], random connectivity [5], or anisotropy [6,7].

In our study we will focus on the effect of weak disorder in the form of random sites. In the simplest case, such disorder may be considered as uncorrelated, randomly distributed pointlike defects. The relevance of pointlike disorder for critical behavior is predicted by the Harris criterion [8]: It changes the universality class of d-dimensional systems if the heat capacity critical exponent α_{pure} of the corresponding homogenous (pure) system is positive. Since in $d = 3$ the pure Ising model has $\alpha_{\text{pure}} > 0$, weak pointlike disorder there leads to a new critical behavior. Results of analytical, numerical, and experimental studies of this celebrated system are reviewed in Ref. [2].

Many real systems contain more complex forms of disorder, for instance, dislocations, disordered layers, grain boundaries, cavities, or other extended defects. To take this into account Weinrib and Halperin have proposed a model [9] in which defects are correlated with a correlation function decaying with distance x according to a power law: $g(x) \sim x^{-a}$. There is possible interpretation for the integer value of a: The case $a = d - 1$ ($a = d - 2$) describes lines (planes) of random orientation, while $a = d$ corresponds to the above-mentioned uncorrelated defects. The critical properties of such systems have been extensively studied by the renormalization group (RG) approach [9–12] as well as through Monte Carlo (MC) simulations [13–15].

Another possible implementation of extended defects was proposed by Dorogovtsev [16] within the model of a d-dimensional spin system with quenched random impurities that are strongly correlated in ε_d dimensions and randomly distributed over the remaining d-ε_d dimensions. In contrast to the model of Weinrib and Halperin which is isotropic [9], Dorogovtsev's model describes a system which is expected to behave differently along the directions "parallel" to the ε_d-dimensional impurity and in the "perpendicular" hyperplanes. The case $\varepsilon_d = 0$ corresponds to pointlike defects, and extended parallel linear (planar) defects are respectively given by $\varepsilon_d = 1(2)$. Generalization of ε_d to non-negative real numbers may be interpreted as an effective fractal dimension of a complex random defect system. However, the relation of analytically continuation to noninteger Euclidean dimension and a fractal dimension is not straightforward [17]. Critical behavior of these systems was extensively studied by RG methods with the help of double $\varepsilon = 4 - d$, ε_d expansions [16,18] as well as applying a resummation technique to the RG asymptotic series directly at $d = 3$ and fixed ε_d [19–22]. There exist also investigations in the mean-field approximation [23] as well as MC simulations which have some connections with Dorogovtsev's model with Ising spins and extended defects with $\varepsilon_d = 2$ [24,25]. In these latter studies, disorder was modeled by random bonds between planes of spins.

In this paper we will consider the critical behavior of the Ising model with parallel linear extended defects in

dimension $d = 3$. Being of considerable interest from the fundamental point of view, such a model describes experimentally achievable situations and may be realized, e.g., as a magnetic film with cylindrical nonmagnetic defects. Such defects (nanopores) might be produced using focused ion or electron beams [26]. To our best knowledge, the model with parallel linear extended defects in dimension $d = 3$ has not been studied numerically so far, although the existing analytical predictions are accurate enough to challenge MC verification. Therefore we present such MC study in our paper. The aim of this paper is therefore precisely to report such an extended numerical study.

The paper is organized as follows. In the next section we briefly present the analytical predictions for scaling of a three-dimensional (3D) system with parallel extended defects as well as the RG estimates for the critical exponents of the Ising system with randomly distributed parallel linear defects. In Sec. III we note the essentials of anisotropic finite-size scaling. The formulation of our model, the definition of the observables, as well as the details of the simulations are listed in Sec. IV. We present the results of simulations in Sec. V, and Sec. VI summarizes our study.

II. ANALYTICAL RESULTS FOR A SPIN MODEL WITH EXTENDED DEFECTS

The critical behavior of the model under consideration is described by the following effective Hamiltonian:

$$\mathcal{H} = \int d^d x \left(\frac{1}{2} \{ \mu_0^2 + V(x) \vec{\phi}^{\,2}(x) + [\nabla_\perp \vec{\phi}(x)]^2 + \alpha_0 [\nabla_{||} \vec{\phi}(x)]^2 \} + \frac{u_0}{4!} [\vec{\phi}^{\,2}(x)]^2 \right). \quad (1)$$

Here $\vec{\phi}$ is an m-component vector field: $\vec{\phi} = \{\phi^1 \cdots \phi^m\}$ (below we will be mainly interested in the Ising case $m = 1$), μ_0 and u_0 are the bare mass and the coupling of the magnetic model, α_0 is the bare anisotropy constant, and $V(x)$ represents the impurity potential, which is assumed to be Gaussian distributed with zero mean and correlator:

$$\overline{V(x)V(x')} = -v_0 \delta^{d-\varepsilon_d}(x_\perp - x'_\perp). \quad (2)$$

Here the overline denotes the average over the potential distribution and $(-v_0)$ is a positive constant proportional to both the concentration of impurities and the strength of their potential. The impurities are envisaged as ε_d-dimensional objects, each extending throughout the system along the coordinate directions symbolized as $x_{||}$, whereas in the remaining d-ε_d dimensions they are randomly distributed. Operators $\nabla_\perp$ and $\nabla_{||}$ mean differentiation in the coordinates $x_\perp$ and $x_{||}$, correspondingly. One assumes that the linear size of the defects is much larger than the spin-correlation length and also larger than the linear separation between any pair of defects. This assumption is valid for defect concentrations well below the percolation threshold.

The static critical behavior [16,18–22] of this model as well as critical dynamics near equilibrium [19,22,27,28] were examined by means of the RG method. A double expansion in both ε, ε_d was suggested and RG functions were calculated to the first order [16]. These results were consistent with a crossover to a new universality class in the presence of extended defects. These calculations were extended to the second order in Ref. [18]. Here it was argued that the Harris criterion is modified in the presence of extended impurities: Randomness is relevant if

$$\varepsilon_d > d - \frac{2}{\nu_{\text{pure}}}, \quad (3)$$

where ν_{pure} is the correlation length critical exponent of the pure system. For pointlike defects ($\varepsilon_d = 0$) Eq. (3) reproduces the usual Harris criterion. A resummation technique applied to the RG asymptotic series [19–22] led to reliable estimates of the critical exponents for this model. Furthermore, different scenarios for the effective critical behavior were discussed [22]. Within the RG approach, the influence of cubic anisotropy of the order parameter [29] and the effect of replica symmetry breaking on the disorder average [30] were studied. Reports of short-time critical dynamics in systems with extended defects are also available in the literature [31]. For completeness, we also mention here several other papers where models with more complex forms of disorder, including extended defects as a particular case, were analyzed [32,33].

The model described by the effective Hamiltonian (1) has rich scaling behavior. As already mentioned, such a system is no longer isotropic. Due to the spatial anisotropy, two correlation lengths exist, one perpendicular and one parallel to the extended impurities direction: $\xi_\perp$ and $\xi_{||}$. As the critical temperature T_c is approached, their divergences are characterized by corresponding critical exponents $\nu_\perp$, $\nu_{||}$:

$$\xi_\perp \sim |t|^{-\nu_\perp}, \quad \xi_{||} \sim |t|^{-\nu_{||}}, \quad (4)$$

where t is the reduced distance to the critical temperature $t = (T - T_c)/T_c$. The correlation of the order parameter fluctuations in two different points acquires an orientational dependence [16]. Thus, the critical exponents $\eta_\perp$ and $\eta_{||}$, which characterize the behavior of the correlation function in the directions perpendicular and parallel to the extended defects, must be distinguished. Spatial anisotropy also modifies the critical dynamics near equilibrium producing two dynamical exponents: $z_{||}$ and $z_\perp$ [27]. On the other hand, as far as the interaction of all order parameter components with defects is the same, the system susceptibility is isotropic in the order parameter space [16] and can be expressed by the pair correlation function [29]:

$$\begin{aligned} \chi(k_\perp, k_{||}, t) &= |t|^{-\gamma} g\left(\frac{k_\perp}{|t|^{\nu_\perp}}, \frac{k_{||}}{|t|^{\nu_{||}}}, \pm 1 \right) \\ &= k_\perp^{\eta_\perp - 2} g_\perp \left(1, \frac{k_{||}}{k_\perp^{\nu_{||}/\nu_\perp}}, \frac{|t|}{k_\perp^{1/\nu_\perp}} \right) \\ &= k_{||}^{\eta_{||} - 2} g_{||} \left(\frac{k_\perp}{k_{||}^{\nu_\perp/\nu_{||}}}, 1, \frac{|t|}{k_{||}^{1/\nu_{||}}} \right). \end{aligned} \quad (5)$$

In Eq. (5), $k_{||}$, $k_\perp$ are the components of the momenta along ε_d and d-ε_d directions, respectively; γ is the magnetic susceptibility critical exponent; and g, $g_\perp$, and $g_{||}$ are the scaling functions. The following scaling relations hold [18,19,29]:

$$\gamma = (2 - \eta_\perp)\nu_\perp = (2 - \eta_{||})\nu_{||}. \quad (6)$$

The critical exponent α of the specific heat is related to $\nu_\perp$, $\nu_{||}$ by the hyperscaling relation that differs from the ordinary one [16]:

$$\alpha = 2 - (d - \varepsilon_d)\nu_\perp - \varepsilon_d \nu_{||}. \quad (7)$$

All the other scaling relations are of the standard form. This implies that one should calculate at least three independent static exponents (e.g., $\nu_{||}, \nu_\perp, \gamma$) instead of two, as in the standard case, to find the other static exponents by scaling relations.

We are mostly interested in the case of Ising spins $m = 1$ and linear parallel extended defects $\varepsilon_d = 1$. For this case we list below the numerical estimates of critical exponents obtained within RG approaches. These estimates based on $\sqrt{\varepsilon}$ expansions are as follows [19]:

$$\nu_\perp = 0.67,\ \nu_{||} = 0.84,\ \gamma = 1.34,\ z_\perp = 2.67,\ z_{||} = 2.22. \quad (8)$$

More reliable estimates are obtained with help of resummation of two-loop RG functions for static exponents [21]:

$$\nu_\perp = 0.750, \quad \nu_{||} = 0.880, \quad \gamma = 1.483, \quad (9)$$

and for dynamic exponents [22]:

$$z_\perp = 2.418, \quad z_{||} = 2.217. \quad (10)$$

It is desirable to check these results with MC simulations. In the following section we show how finite-size scaling may be used to extract quantitative characteristics of the critical behavior from MC data obtained for finite systems.

III. ANISOTROPIC FINITE-SIZE SCALING

Systems studied by MC simulations have limited sizes. Therefore finite-size scaling (FSS) [34–38] plays a key role in extracting the critical exponents of thermodynamical functions from MC data. According to FSS theory, in the vicinity of the critical point $t \to 0$, the order parameter M and the susceptibility χ of isotropic systems scale with the linear size L as:

$$M(t \to 0) = L^{-\beta/\nu}\mathcal{M}(L), \quad (11)$$

$$\chi(t \to 0) = L^{\gamma/\nu}\tilde{\chi}(L), \quad (12)$$

where $\mathcal{M}$, $\tilde{\chi}$ are magnetization and susceptibility scaling functions. There is no dependence on the direction on the lattice in this case (the x, y, and z directions are equivalent for the three-dimensional model). A quantity of special interest often used within MC simulations, namely the fourth-order Binder cumulant [39], obeys the following behavior:

$$U_4(t, L) = 1 - \frac{\langle M^4 \rangle}{3\langle M^2 \rangle^2} = \tilde{U}_4(tL^{1/\nu}), \quad (13)$$

where $\langle M^2 \rangle$, $\langle M^4 \rangle$ are second and fourth moments of the distribution of order parameters, and $\tilde{U}_4$ is the scaling function. In isotropic models all curves of the temperature dependence of U_4 for different system sizes intersect in one point, indicating the location of the critical temperature. It is true even if one keeps different aspect ratios for the simulation box: The curves for different sizes at a given generalized aspect ratio all intersect in the thermodynamic limit at the critical temperature [40].

There exist different systems that manifest strong anisotropic scaling at criticality, i.e., the critical exponents for their correlation lengths differ in different directions. Among them we mention as examples the behavior of the next-nearest-neighbor Ising model at the Lifshitz point [41], nonequilibrium phase transition in driven diffusive systems [42], the dipolar in-plane Ising model [43], the driven Ising model with friction [44], the Ising model under shear [45,46], and the interface localization-delocalization problem [47]. A common feature of the above-mentioned systems is the presence a single anisotropy axis which results in the existence of two characteristic length scales: $L_{||}$ along the anisotropy axis and $L_\perp$ in the perpendicular directions. According to the generalization of the FSS concept for systems with two characteristic length scales [48], the properties of the thermodynamical functions depend on the "generalized aspect ratio" $\rho = L_{||}/L_\perp^\theta$, with an anisotropy exponent $\theta = \nu_{||}/\nu_\perp$. Therefore relations (11) and (12) are modified:

$$M(t \to 0) = L_{||}^{-\beta/\nu_{||}}\mathcal{M}_{||}(L_{||}/L_\perp^\theta), \quad (14)$$

$$\chi(t \to 0) = L_{||}^{\gamma/\nu_{||}}\tilde{\chi}_{||}(L_{||}/L_\perp^\theta). \quad (15)$$

Note that (14) and (15) can be equivalently represented as:

$$M(t \to 0) = L_\perp^{-\beta/\nu_\perp}\mathcal{M}_\perp(L_\perp/L_{||}^{1/\theta}), \quad (16)$$

$$\chi(t \to 0) = L_\perp^{\gamma/\nu_\perp}\tilde{\chi}_\perp(L_\perp/L_{||}^{1/\theta}), \quad (17)$$

where scaling functions $\mathcal{M}_{||}(\rho) = \rho^{-\beta/\nu_{||}}\mathcal{M}_\perp(\rho^{-1/\theta})$ and $\tilde{\chi}_{||}(\rho) = \rho^{\gamma/\nu_{||}}\tilde{\chi}_\perp(\rho^{-1/\theta})$. Anisotropic finite-size scaling for the Binder cumulant at the critical point predicts

$$U_4(t \to 0) = \tilde{U}_4(L_{||}/L_\perp^\theta). \quad (18)$$

Therefore, one has to keep the generalized aspect ratio $L_{||}/L_\perp^\theta$ fixed while performing MC simulations to extract critical exponents. One can use the values of the exponents (8)–(10) to evaluate the anisotropy exponent θ for the model under consideration. Using the results of $\sqrt{\varepsilon}$ expansions (8) we can estimate $\theta = \nu_{||}/\nu_\perp \simeq 1.25$. Taking into account that $\nu_{||}/\nu_\perp = z_\perp/z_{||}$ [19], we can get the second estimate of the $\sqrt{\varepsilon}$ expansions: $\theta = z_\perp/z_{||} \simeq 1.20$. Other estimates can be obtained with help of the results of resummation of two-loop RG functions: $\theta = \nu_{||}/\nu_\perp = 1.173$ from (9) and $\theta = z_\perp/z_{||} = 1.091$ from (10). All estimates give $\theta > 1$. This reflects the physical situation: In parallel directions, the fluctuations are stronger because they are not limited by defects and the correlation length in this direction diverges more sharply.

In order to obtain an estimate of θ directly from the MC simulations, independently of the RG predictions, we can make use of the relation that characterizes systems possessing anisotropic scaling when $L_\perp \gg L_{||}$ at $t \to 0$ [43,49]:

$$\xi_\perp(L_{||}) \sim L_{||}^{1/\theta}. \quad (19)$$

Such a relation was successfully applied for the analysis of the second-order phase transitions in Ising models with friction [44] and under shear [46].

In the following sections, we use the formulas (14)–(19) to perform the analysis of the results of MC simulations.

IV. DETAILS OF THE SIMULATIONS

We consider the 3D Ising model on a simple cubic lattice of $L_\perp \times L_\perp \times L_{||} = V$ sites. Each site $i = (x,y,z)$, $1 \leqslant x \leqslant L_\perp$, $1 \leqslant y \leqslant L_\perp$, $1 \leqslant z \leqslant L_{||}$, is characterized by the occupation number $c_i = \{0,1\}$ with $c_i = 1$ if the site i is occupied by a spin $s_i = \pm 1$, while $c_i = 0$ corresponds to a nonmagnetic site i. Nearest-neighbor spins interact ferromagnetically with constant exchange $J > 0$. Explicitly, the Hamiltonian of the model may be written as

$$\mathcal{H} = -J \sum_{\langle i,j \rangle} c_i c_j s_i s_j, \tag{20}$$

where the sum $\langle i,j \rangle$ is taken over the pairs of nearest-neighbor spins. We use periodic boundary conditions.

The nonmagnetic sites ($c_i = 0$) in our model have to be arranged into parallel lines and oriented along a given axis, say the z axis. The length of these lines coincides with the system size in z direction, $L_{||}$. Figure 1 shows one possible configuration of such lines.

We generate the impurity distribution for a given impurity concentration p for a lattice of size V in the following way. We compute the integer number $n_{\rm imp} = {\rm int}(pL_\perp^2)$ of impurity lines of length $L_{||}$. We distribute randomly intersections of these lines with the x-y plane, as shown in Fig. 1.

We compute powers of the magnetization ($k = 1,2,4$)

$$M^k = \left(\frac{1}{V} \sum_{\{i\}} c_i s_i \right)^k, \tag{21}$$

where $\{i\}$ means the lattice summation over all sites. From powers of the magnetization we construct the magnetic susceptibility and Binder cumulant in the following way:

$$\chi = \beta V \overline{(\langle M^2 \rangle - \langle |M| \rangle^2)}, \tag{22}$$

$$U_4 = 1 - \overline{\left(\frac{\langle M^4 \rangle}{3 \langle M^2 \rangle^2} \right)}. \tag{23}$$

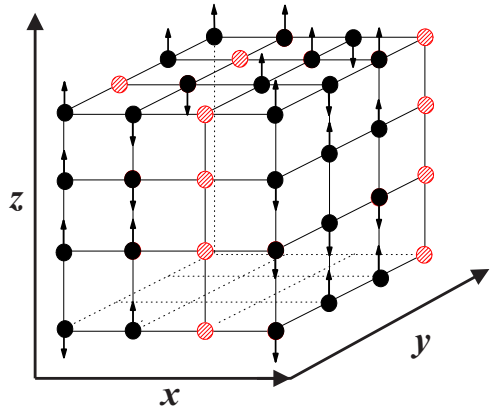

FIG. 1. (Color online) An example of the lattice of size $4 \times 4 \times 4$ with Ising spins (dark circles) and nonmagnetic impurities (light circles, red online) collected into $n_{\rm imp} = 4$ lines.

Here at first step we perform the thermal averaging of the power of magnetization for each impurity realization (denoted by angle brackets, e.g., $\langle M^2 \rangle$). Then we average these results over impurity realizations. The averaging over impurity realizations is denoted by the overline. In our simulation we fix $J/k_B = 1$, in which case $\beta = 1/T$ is the inverse temperature.

We compute also the correlation lengths for directions parallel to the impurity lines, $\xi_{||}$, and in the perpendicular planes, $\xi_\perp$, with the help of the Fourier transform in a similar way as it was done for isotropic systems [50]. Let us introduce $s(\mathbf{k}) = \sum_j e^{i\mathbf{k}\cdot\mathbf{r}_j} c_j s_j$, where $\mathbf{r}_j = (x,y,z)$ is the radius vector of the spin s_j, the wave vector is $\mathbf{k} = (k_x,k_y,k_z)$, and we denote $\langle \chi_0 \rangle = \langle |s(0,0,0)|^2 \rangle$, $\langle \chi_1^{||} \rangle = \langle |s(0,0,2\pi/L_{||})|^2 \rangle$, and $\langle \chi_1^\perp \rangle = \langle |s(2\pi/L_\perp,0,0)|^2 \rangle$ thermal average of Fourier components for particular realization of impurities. Then we can compute the corresponding correlation lengths averaged over impurity realizations

$$\xi_{||} = \frac{1}{2\sin(\pi/L_{||})} \sqrt{\overline{\frac{\langle \chi_0 \rangle}{\langle \chi_1^{||} \rangle}} - 1}, \tag{24}$$

$$\xi_\perp = \frac{1}{2\sin(\pi/L_\perp)} \sqrt{\overline{\frac{\langle \chi_0 \rangle}{\langle \chi_1^\perp \rangle}} - 1}. \tag{25}$$

The simulation is performed with hybrid MC method [51]. Each of MC step consists of one flip of Wolff cluster followed by $V/4$ attempts to flip spins in accordance with Metropolis rule. The Wolff cluster update prevents the critical slowing-down while Metropolis single spin flips for the system with impurities should spend a lot of time to provide the update of weakly connected regions.

In our study we deal with a concentration of impurities $p = 0.2$. Such concentration is very often used in MC simulations of an Ising model with disorder [13–15,52], since in this case the concentration of magnetic sites $1 - p = 0.8$ is far from the percolation threshold and from the pure system. An additional empirical reason to take this value of p is the following: For a 3D Ising model with uncorrelated impurities, correction-to-scaling terms were found to be minimal at concentration of magnetic sites 0.8 [52], and in the absence of a more robust argument, we stick to this value in the present work although correlated disorder is obviously a different situation.

V. RESULTS AND ANALYSIS OF SIMULATIONS

In this section, applying the above-described formalism, we give three estimates of the anisotropy exponent obtained from anisotropic FSS predictions for different quantities. From the FSS of susceptibility we get also an estimate for $\gamma/\nu_\perp$.

A. Computation of the correlation length

To use relation (19) we need to perform calculations at a fixed value of the variable $L_{||} t^{\nu_{||}}$, e.g., at the critical temperature of an infinite system. Let us assume that the value of the critical temperature of an infinite system is very close to the value of the pseudocritical temperature of the system with maximal size. In this case that is the temperature of the susceptibility maximum $\chi_{\rm max}$ of the largest system available.

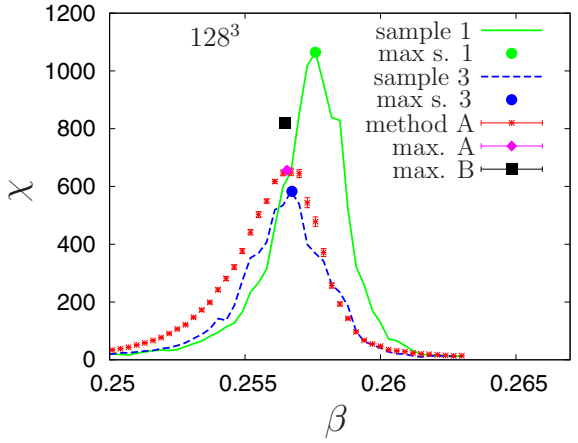

FIG. 2. (Color online) Maxima of magnetic susceptibility χ; $\beta^A_{\max} = 0.25655(10)$ for method A and $\beta^B_{\max} = 0.25648(5)$ for method B for a system 128^3 and $p = 0.2$.

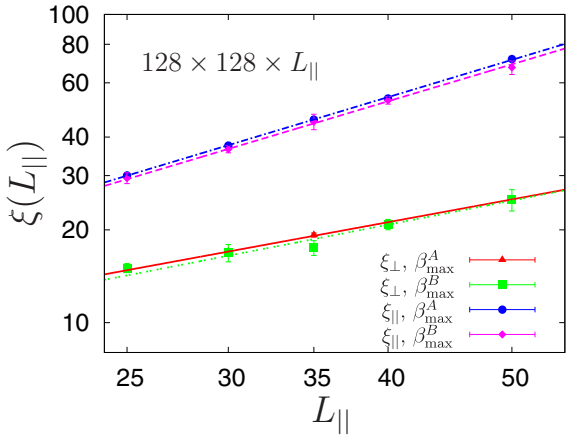

FIG. 3. (Color online) Results of the fit of ξ as a power-law dependence of $L_{||}$ for a system of size $128 \times 128 \times L_{||}$ and $p = 0.2$ at point $\beta^A_{\max} = 0.25655(10)$ for method A and $\beta^B_{\max} = 0.25648(5)$ for method B.

We perform the computation for a cubical system of size 128^3 with concentration of impurities $p = 0.2$. Disorder average may be performed in either of two possible protocols: In the first procedure, we measure the temperature dependence of the susceptibility at each disorder realization. Then all these curves are averaged to get a single curve of χ that depends on β. The value β at which $\chi(\beta)$ has a maximum is then associated with the critical temperature (we refer to this as *method A*). The alternative is to average temperatures at which $\chi_{\max}$ is achieved *for each disorder realization* (we refer to this as *method B*).

The results obtained with both methods are given in Fig. 2. The two curves displayed by continuous lines in the figure show $\chi(\beta)$ behavior for two separate samples, whereas the dotted curve shows the $\chi(\beta)$ averaged over 320 samples. Using method A we first average the susceptibility and then find the point $\beta^A_{\max} = 0.25655(10)$ (magenta diamond in Fig. 2). Using method B we first find a maximum of susceptibility for each disorder configuration and then average location of these maxima over samples $\beta^B_{\max} = 0.25648(5)$ (black square in Fig. 2). These two evaluations for $\beta_{\max}$ for methods A and B coincide within the evaluation of numerical accuracy. Method A corresponds to the averaging of the free energy over the impurity realizations and we shall use this evaluation of the pseudocritical point $\beta^A_{\max} = 0.25655(10)$. With the value of the critical temperature at hand we can perform a study through relation (19) to extract the anisotropy exponent θ. To this end, we analyze the correlation length $\xi_\perp$ of the system of size $128 \times 128 \times L_{||}$, fixing the perpendicular size $L_\perp = 128$ and varying $L_{||}$ for both values of $\beta_{\max}$. Results of simulations for $L_{||} = 25$–50 are given in Fig. 3, where we plot ξ for the $\perp$ and $||$ directions as a function of $L_{||}$.

Then we perform the fit of data for $\xi_\perp$ in accordance with the formula:

$$\xi_\perp(L_{||}) = aL^b_{||}, \tag{26}$$

using fitting parameters a and b. For method A we get $a = 1.27(4)$, $b = 0.76(1)$, while for method B we estimate $a = 1.06(3)$, $b = 0.81(5)$. Comparing (26) with (19), we get $\theta = 1/b$ with the following estimates: $\theta \approx 1.31$ (method A) and $\theta \approx 1.23$ (method B). Taking these values as an accuracy interval of θ, $1.2 \lesssim \theta \lesssim 1.3$ we see that these are in reasonable agreement with the existing analytic RG estimates (see Sec. III).

B. Computation of the Binder cumulant

Another way to identify the right value of the exponent θ is the following. We expect that all curves for the temperature dependence of the Binder cumulant U_4 for systems of different sizes but fixed generalized aspect ratio with proper θ will intersect at the critical point. Therefore we can consider the system of size $L_\perp \times L_\perp \times L_{||}$ and keep the condition $L_{||} = L^\theta_\perp$, but we will perform a series of simulations for various values of θ. For each θ, we compute the cumulant $U_4(\beta, L_\perp)$ as a function of the inverse temperature β for various values of $L_\perp$. At the proper value θ^* we expect the intersection of the curves of Binder cumulants. We perform simulations for $L_\perp = 20, 40, 60, 80, 100$, and the disorder average is performed over $N_{\text{imp}} = 128$ realizations of impurities.

In Figs. 4(a)–4(d) we plot the cumulant for values $\theta = 1, 1.1, 1.2, 1.3$, respectively. Each curve corresponds to $U_4(\beta)$ averaged over 128 disorder realizations. As one can see, the presence of disorder smears the single crossing point into a region of temperatures where all curves cross. The narrowest region is expected for the value of θ which is sufficiently close to the real one. To analyze this situation for different values of θ, we use the following procedure. We split the total set of $N_{\text{imp}} = 128$ different impurity realizations onto eight series and compute the average value (averaged over $128/8 = 16$ realizations) of the invariant U^k_4 for each set $k = 1, 2, \ldots, 8$. Later we use the averaging of U^k_4 for the evaluation of numerical accuracy. In Fig. 5(a) we plot for comparison results for U^k_4 as a function of β for two different series $k = 1$ (lines) and $k = 2$ (triangles) for $\theta = 1$ and various sizes $L_\perp = 20$, 40, 60, 80, 100. In this figure we observe an important difference between the graphs for two series due to fluctuations induced by the presence of impurities. Our aim is to study the scattering of intersection points. Ideally, graphs for five

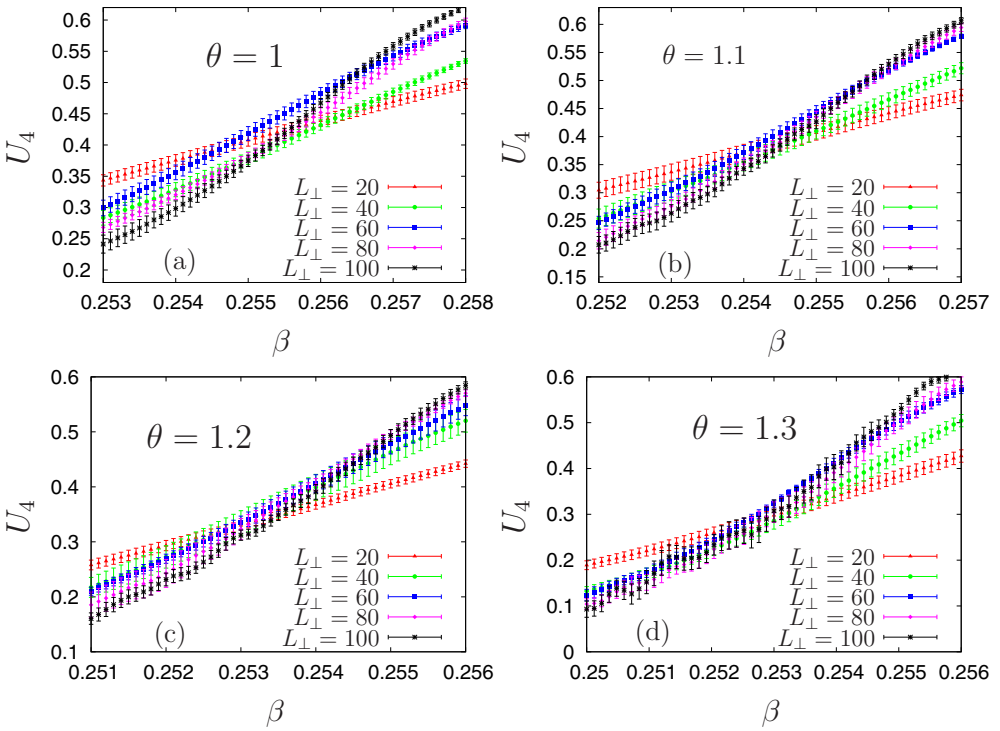

FIG. 4. (Color online) Magnetization cumulant U_4 as a function of the inverse temperature β for different system sizes, keeping the condition $L_{||} = L_\perp^\theta$: (a) $\theta = 1.0$, (b) $\theta = 1.1$, (c) $\theta = 1.2$, and (d) $\theta = 1.3$.

system sizes should intersect in 10 points. In Fig. 5(b) we plot data for $U_4^{k=1}$ and indicate the intersection points (β_{ij}^k, U_{ij}^k) by black circles. Here a pair ij of indexes labels two system sizes $i = 1, 2, 3, 4, 5$ for $L_\perp = 20, 40, 60, 80, 100$. The curves for some of the system sizes have intersections which fall outside of the considered interval for β, e.g., for $L_\perp = 40$ and for $L_\perp = 80, 100$. In this case we select as "intersection point" the point between left side or right side ends of these two lines selecting the side with the smaller distance between the end points.

Another possible situation with multiple intersection points may happen due to a big scattering of the data points caused by numerical inaccuracy. In this case, we perform the averaging over all intersection points and proceed with this averaged point. Then we compute the mean values of the inverse temperature,

$$\beta_{\text{av}}^k = \frac{1}{10} \sum_{i=1}^{5} \sum_{j<i}^{5} \beta_{ij}^k,$$

and of the cumulant,

$$U_{\text{av}}^k = \frac{1}{10} \sum_{i=1}^{5} \sum_{j<i}^{5} U_{ij}^k,$$

over 10 intersection points for five system sizes for each set k. We observe (as expected), that the average of crossing points does not coincide with the crossing of average lines.

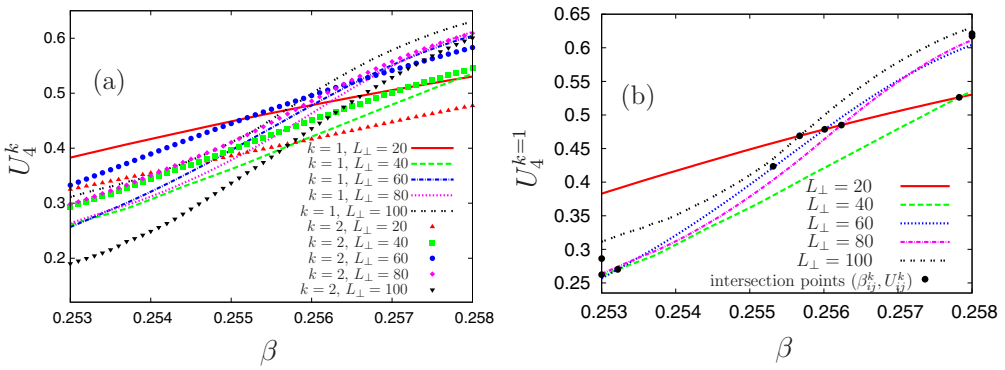

FIG. 5. (Color online) The cumulant U_4^k for the k-th series as a function of β for $\theta = 1$ and various values of $L_\perp = 20, 40, 60, 80, 100$: (a) Comparison of results for $k = 1$ (lines) and $k = 2$ (symbols). Note that some pair of graphs (for example, for $L_\perp = 40$ and $L_\perp = 80, 100$ for $k = 1$) have no intersection within the considered range. (b) Results for $k = 1$ and intersection points (β_{ij}^k, U_{ij}^k).

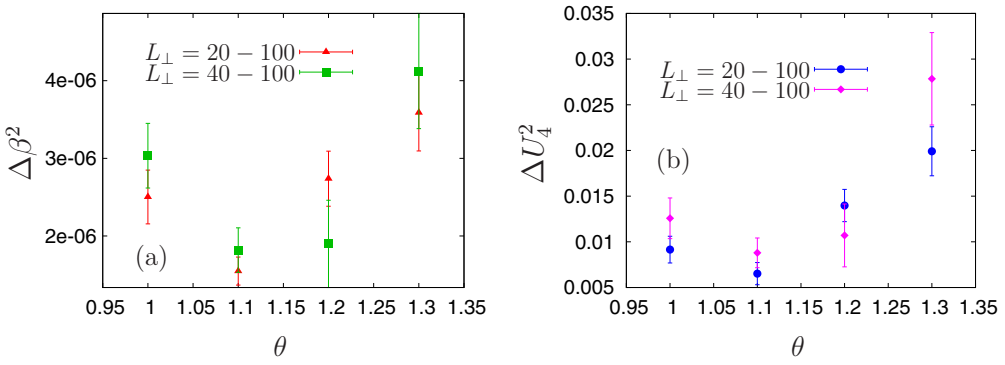

FIG. 6. (Color online) (a) The average of the square deviation of the inverse temperature $\Delta\beta^2$ of crossing points as a function of θ; (b) the average of the square deviation of the cumulant ΔU_4^2 of crossing points as a function of θ.

Now we can compute the average values of the deviations squared from the mean values for the inverse temperature,

$$\Delta\beta^2 = \frac{1}{8\times 10}\sum_{k=1}^{8}\sum_{i=1}^{5}\sum_{j<i}^{5}\left(\beta_{ij}^k - \beta_{\rm av}^k\right)^2,$$

and for the cumulant,

$$\Delta U_4^2 = \frac{1}{8\times 10}\sum_{k=1}^{8}\sum_{i=1}^{5}\sum_{j<i}^{5}\left(U_{ij}^k - U_{\rm av}^k\right)^2,$$

and evaluate numerical accuracy. In Fig. 6(a) we plot $\Delta\beta^2$ as a function of θ.

The amplitude of the square of the inverse temperature deviation is about 10^{-6}, which is consistent with the average distance between points $\Delta\beta \sim 10^{-3}$. We do not observe pronounced minima in the interval $1.0 \leqslant \theta \leqslant 1.3$, and the numerical inaccuracy is comparable with the scattering of the points. In Fig. 6(b) we plot data for the average square of the deviation for the cumulant ΔU_4^2. The point distribution is very similar to the ones obtained for the inverse temperature. The point for $\theta = 1.1$ is below its neighbors, but the distance between these points is of the order of the numerical accuracy. Therefore the procedure corroborates $\theta = 1.1$ as the optimal one.

C. Computations of the susceptibility

In this subsection we describe the results of the computation of the magnetic susceptibility at the critical point β_c with various values of the exponent θ. In Fig. 7 we plot the magnetic susceptibility χ as a function of the system size $L_\perp$ in the log-log scale for $\beta_{\rm max}^A = 0.25655(10)$.

We perform a fit of the magnetic susceptibility by a linear function of $L_\perp$ in the log-log scale: $\chi = aL_\perp^b$ with a and b being the parameters of the fit. Then we estimate the deviation of the values of susceptibility measured numerically from those obtained via the fitting function with the help of a $\hat{\chi}^2$ defined as

$$\hat{\chi}^2 = \sum_{i=1}^{N}\frac{[\chi_i - f(L_i)]^2}{\sigma_i^2}. \tag{27}$$

Here $N = 8$ is the number of values χ_i calculated for $i = 1,2,\ldots,N$ values of $L_{\perp i} = 10,20,30,40,50,60,80,100$; $f(x)$ is the fitting function; and σ_i^2 is the appropriate variance defined by the error bars.

The same number of MC steps is used for a given value of the exponent θ. Therefore, the variance σ_i is minimal for small values of the system size $L_\perp$ and increases for larger values of $L_\perp$. The total number of MC steps decreases with increasing of θ (from 5×10^6 for $\theta = 1$ to 5×10^5 for $\theta = 1.45$).

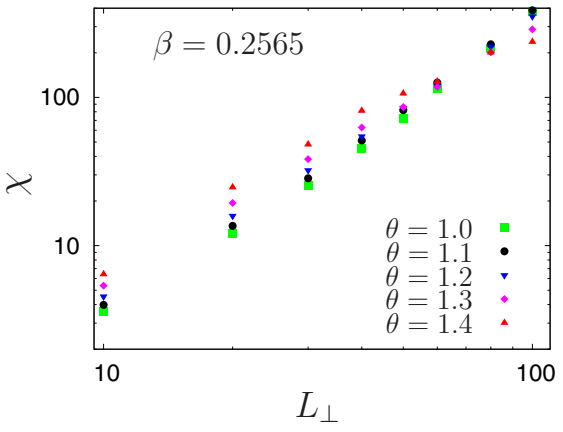

FIG. 7. (Color online) Magnetic susceptibility χ as a function of the system size $L_\perp$ for various values of $\theta = 1$, 1.1, 1.2, 1.3, 1.4 at the point $\beta_{\rm max}^A = 0.25655(10)$.

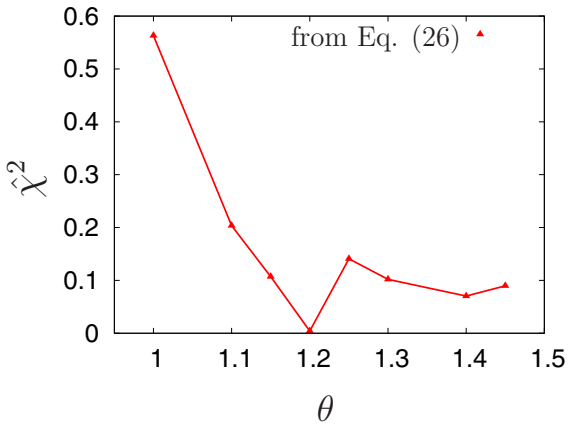

FIG. 8. (Color online) The $\hat{\chi}^2$ parameter of the deviation from the linear fit [Eq. (27)] of the magnetic susceptibility as a function of θ.

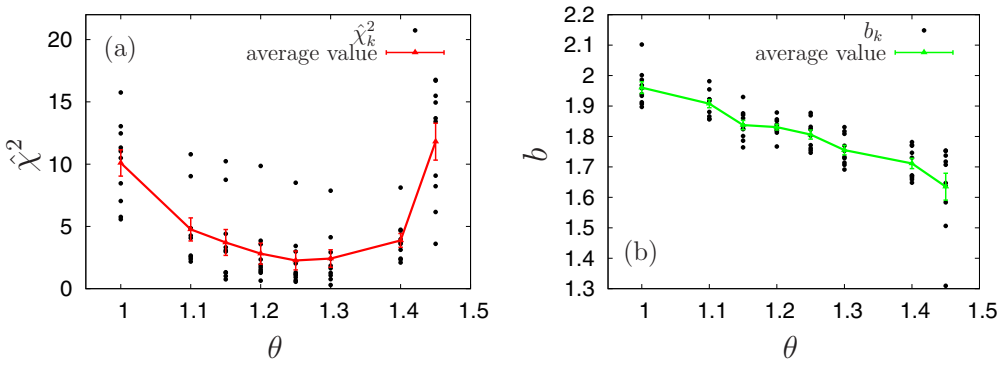

FIG. 9. (Color online) (a) The $\hat{\chi}^2$ parameter of the linear fit with variance ($\hat{\chi}^2_k$ for every series, black circles; average result, red triangles) as a function of θ; (b) the result of the power of the fit b (b_k for every series, black circles; average result, green triangles) as a function of θ.

The parameter $\hat{\chi}^2$ of the fitting procedure characterizes the "quality" of the data with respect to the proposed functional dependence. In our case this parameter describes the deviation of points from the straight line in the log-log representation. We plot $\hat{\chi}^2$ as a function of θ in Fig. 8. The general tendency is the decrease of $\hat{\chi}^2$ with an increase of θ. This is due to the larger variance when the number of MC steps is smaller.

We observe a minimum in the region $\theta \approx 1.2$–1.3. Unfortunately, for this procedure we cannot evaluate the variance (inaccuracy) $\delta\hat{\chi}^2$. Therefore we repeat the procedure, splitting the 320 disorder realizations (for each value of $L_\perp$ for a fixed θ) into 10 series and perform the fit by the formula $\ln(\chi) \simeq \ln(a_k) + b_k \ln(L_\perp)$ for every series obtaining some value $\hat{\chi}^2_k$. Then we average these values, compute numerical accuracy, and plot the results in Fig. 9(a) (black circles for $\hat{\chi}^2_k$ and red triangles for the average value). We can see that $\hat{\chi}^2$ reaches the minimum for $\theta^* \simeq 1.25$. In Fig. 9(b) we plot the resulting exponent b as a function of θ. The value of b at θ^* gives an estimate for $\gamma/\nu_\perp \simeq 1.85 \pm 0.05$, using the window $1.1 \leqslant \theta \leqslant 1.3$. We present here also the estimate $\gamma/\nu_\perp = 1.90 \pm 0.08$ obtained from data of Fig. 9 for the value $\theta = 1.1$ recognized as an optimal value in Sec. V B in the cumulant analysis.

VI. CONCLUSION

In this paper we have studied by use of MC simulations the scaling behavior of thermodynamical quantities in the vicinity of critical point for a 3D Ising system with randomly distributed parallel linear extended defects, modeled as nonmagnetic impurities collected into lines along spatial direction z. We considered a combined algorithm using the Wolff and Metropolis methods. Our results are consistently interpreted using the theory of anisotropic finite-size scaling.

We have estimated the value of the anisotropy exponent θ using three different methods, namely from dependence of correlation length $\xi_\perp$ on the linear size of the system near the critical point, from a temperature dependence of the fourth-order Binder cumulant, and from finite-size scaling of the susceptibility. The values estimated are in the range $1.1 \leqslant \theta \leqslant 1.3$ and corroborate RG predictions for the model under consideration.

We have also measured the value of $\gamma/\nu_\perp$ from anisotropic finite-size scaling for the susceptibility. The value reported here $\gamma/\nu_\perp \simeq 1.85$ is a little bit below the corresponding RG estimates $\gamma/\nu_\perp \simeq 2.0$, $\gamma/\nu_\perp \simeq 1.98$. The value $\gamma/\nu_\perp \simeq 1.9$ estimated for $\theta = 1.1$ is in better agreement with theoretical results. We have applied the procedure described in Sec. V for susceptibility to compute the magnetization. However, it does not give satisfactory results in this case. This is because magnetization is a vanishing quantity at the critical point and therefore it is very sensitive to proper determination of critical temperature.

Finally, let us mention that in spite of the substantial computation effort reported in this paper, the numerical values of the critical exponents are not extremely accurate. This is due to the difficulty of the numerical techniques to deal with anisotropic systems (see, e.g., Ref. [53]), but from the MC simulations presented in this paper, we believe that we can safely conclude in favor of the anisotropic critical point, since anisotropic scaling is overall nicely confirmed.

ACKNOWLEDGMENTS

This work was supported in part by the European Union's Research and Innovation funding programme FP7 IRSES Marie-Curie Grant No. PIRSES-GA-2010-269139 "Dynamics and Cooperative Phenomena in Complex Physical and Biological Environments" and No. PIRSES-GA-2011-295302 "Statistical Physics in Diverse Realizations." M.D. acknowledges Oleg Vasilyev and his colleagues for their hospitality during his stay in the Max Planck Institute for Intelligent Systems (Stuttgart).

[1] *Order, Disorder and Criticality*, edited by Yu. Holovatch (World Scientific, Singapore, 2004); Yu. Holovatch, V. Blavats'ka, M. Dudka, C. von Ferber, R. Folk, and T. Yavors'kii, Int. J. Mod. Phys. B **16**, 4027 (2002).

[2] For recent reviews on criticality of diluted magnets see, e.g., A. Pelissetto and E. Vicari, Phys. Rep. **368**, 549 (2002); R. Folk, Yu. Holovatch, and T. Yavorskii, Phys.-Usp. **46**, 169 (2003) [Usp. Fiz. Nauk. **173**, 175 (2003)].

[3] P. E. Berche, C. Chatelain, B. Berche, and W. Janke, Eur. Phys. J. B **38**, 463 (2004); B. Berche, P. E. Berche, C. Chatelain, and W. Janke, Condens. Matter Phys. **8**, 47 (2005).

[4] D. P. Belanger and A. P. Young, J. Magn. Magn. Mater. **100**, 272 (1991).

[5] W. Janke and M. Weigel, Phys. Rev. B **69**, 144208 (2004); J. M. Luck, Europhys. Lett. **24**, 359 (1993).

[6] A review of early work on random anisotropy magnets may be found in: R. W. Cochrane, R. Harris, and M. J. Zuckermann, Phys. Rep. **48**, 1 (1978). More recent experimental, numerical, and theoretical studies are reviewed in Ref. [7].

[7] M. Dudka, R. Folk, and Yu. Holovatch, J. Mag. Mag. Mat. **294**, 305 (2005).

[8] A. B. Harris, J. Phys. C **7**, 1671 (1974).

[9] A. Weinrib and B. I. Halperin, Phys. Rev. B **27**, 413 (1983).

[10] E. R. Korutcheva and D. I. Uzunov, Phys. Stat. Sol. (b) **126**, K19 (1984); E. Korutcheva and F. Javier de la Rubia, Phys. Rev. B **58**, 5153 (1998).

[11] V. V. Prudnikov, P. V. Prudnikov, and A. A. Fedorenko, J. Phys. A **32**, L399 (1999); **32**, 8587 (1999); Phys. Rev. B **62**, 8777 (2000).

[12] V. Blavats'ka, C. von Ferber, and Yu. Holovatch, Phys. Rev. E **64**, 041102 (2001); for recent papers see, V. Blavatska, C. von Ferber, and Yu. Holovatch, *ibid.* **83**, 011803 (2011), and references therein.

[13] H. G. Ballesteros and G. Parisi, Phys. Rev. B **60**, 12912 (1999).

[14] V. V. Prudnikov, P. V. Prudnikov, S. V. Dorofeev, and V. Yu. Kolesnikov, Condens. Matter Phys. **8**, 213 (2005); V. Prudnikov, P. Prudnikov, B. Zheng, S. Dorofeev, and V. Kolesnikov, Progr. Theor. Phys. **117**, 973 (2007).

[15] D. Ivaneyko, B. Berche, Yu. Holovatch, and J. Ilnytskyi, Physica A **387**, 4497 (2008).

[16] S. M. Dorogovtsev, Fiz. Tverd. Tela (Leningrad) **22**, 321 (1980) [Sov. Phys. Solid. State **22**, 188 (1980)]; Fiz. Tverd. Tela (Leningrad) **22**, 3659 (1980) [Sov. Phys. Solid. State **22**, 2141 (1980)].

[17] Y. Gefen, B. B. Mandelbrot, and A. Aharony, Phys. Rev. Lett. **45**, 855 (1980); Y. K. Wu and B. Hu, Phys. Rev. A **35**, 1404 (1987); Yu. Holovatch, Lecture Notes in Physics, Vol. 447 (Springer-Verlag, Heidelberg, 1996), p. 224; Yu. Holovatch and N. Shpot, J. Stat. Phys. **66**, 867 (1992); Yu. Holovatch and T. Yavors'kii, *ibid.* **92**, 785 (1998).

[18] D. Boyanovsky and J. L. Cardy, Phys. Rev. B **26**, 154 (1982); **27**, 6971(E) (1983).

[19] I. D. Lawrie and V. V. Prudnikov, J. Phys. C **17**, 1655 (1984).

[20] V. Blavats'ka, C. von Ferber, and Yu. Holovatch, Acta Physica Slovaca **52**, 317 (2002).

[21] V. Blavats'ka, C. von Ferber, and Yu. Holovatch, Phys. Rev. B **67**, 094404 (2003).

[22] V. Blavats'ka, M. Dudka, R. Folk, and Yu. Holovatch, Phys. Rev. B **72**, 064417 (2005).

[23] B. Berche, P. E. Berche, F. Iglói, and G. Palagyi, J. Phys. A: Math. Gen. **31**, 5193 (1998).

[24] J. C. Lee and R. L. Gibbs, Phys. Rev. B **45**, 2217 (1992).

[25] T. Vojta, J. Phys. A: Math. Gen. **36**, 10921 (2003); R. Sknepnek and T. Vojta, Phys. Rev. B **69**, 174410 (2004).

[26] C. J. Lo, T. Aref, and A. Bezryadin, Nanotechnology **17**, 3264 (2006).

[27] V. V. Prudnikov, J. Phys. C **16**, 3685 (1983).

[28] V. Blavatska, M. Dudka, R. Folk, and Yu. Holovatch, J. Mol. Liq. **127**, 60 (2006).

[29] Y. Yamazaki, A. Holz, M. Ochiai, and Y. Fukuda, Physica A **150**, 576 (1988); Phys. Rev. B **33**, 3460 (1986); Y. Yamazaki, Y. Fukuda, A. Holz, and M. Ochiai, Physica A **136**, 303 (1986); Y. Yamazaki, M. Ochiai, A. Holz, and Y. Fukuda, Phys. Rev. B **33**, 3474 (1986).

[30] L. De Cesare and M. T. Mercado, Phys. Rev. B **59**, 855 (1999).

[31] A. A. Fedorenko, Phys. Rev. B **69**, 134301 (2004).

[32] L. De Cesare, Phys. Rev. B **49**, 11742 (1994); L. De Cesare and M. T. Mercado, Phys. Lett. A **186**, 179 (1994); **264**, 214 (1994).

[33] A. L. Korzhenevskii, K. Herrmanns, and W. Schirmacher, Phys. Rev. B **53**, 14834 (1996).

[34] M. E. Fisher, in *Critical Phenomena*, edited by M. S. Green (Academic, New York, 1971).

[35] M. E. Fisher and M. N. Barber, Phys. Rev. Lett. **28**, 1516 (1972).

[36] M. N. Barber, in *Phase Transitions and Critical Phenomena*, edited by C. Domb and J. Lebowitz (Academic, New York, 1983), Vol. 8.

[37] V. Privman, in *Finite Size Scaling and Numerical Simulations of Statistical Systems Phase Transitions and Critical Phenomena*, edited by V. Privman (Singapore, World Scientific, 1990).

[38] V. Privman and M. E. Fisher, Phys. Rev. B **30**, 322 (1984).

[39] K. Binder, Z. Phys. B **43**, 119 (1981).

[40] K. Kaneda, Y. Okabe, and M. Kikuchi, J. Phys. A **32**, 7263 (1999).

[41] H. W. Diehl and M. Shpot, Phys. Rev. B **62**, 12338 (2000).

[42] J.-S. Wang, J. Stat. Phys. **82**, 1409 (1996); K. Leung and J.-S. Wang, Int. J. Mod. Phys. C **10**, 853 (1999); K.-T. Leung, *ibid.* **03**, 367 (1992); K. Leung and J. L. Cardy, J. Stat. Phys. **44**, 567 (1986).

[43] A. Hucht, J. Phys. A **35**, L481 (2002).

[44] A. Hucht, Phys. Rev. E **80**, 061138 (2009); S. Angst, A. Hucht, and D. E. Wolf, *ibid.* **85**, 051120 (2012).

[45] D. Winter, P. Virnau, J. Horbach, and K. Binder, Europhys. Lett. **91**, 60002 (2010).

[46] A. Hucht and S. Angst, Europhys. Lett. **100**, 20003 (2012).

[47] A. Milchev, M. Müller, K. Binder, and D. P. Landau, Phys. Rev. Lett. **90**, 136101 (2003).

[48] K. Binder and J.-S. Wang, J. Stat. Phys. **55**, 87 (1989).

[49] M. Henkel and U. Schollwöck, J. Phys. A **34**, 3333 (2001).

[50] F. Cooper, B. Freedman, and D. Preston, Nucl. Phys. B **210**, 210 (1989).

[51] D. P. Landau and K. Binder, *A Guide to Monte Carlo Simulations in Statistical Physics* (Cambridge University Press, London, 2005), p. 155.

[52] H. G. Ballesteros, L. A. Fernández, V. Martín-Mayor, A. Muñoz Sudupe, G. Parisi, and J. J. Ruiz-Lorenzo, Phys. Rev. B **58**, 2740 (1998).

[53] C. Chatelain, P. E. Berche, and B. Berche, Eur. Phys. J. B **7**, 439 (1999).